Field Emission of Electrons Generated by the Near Field of Strongly Coupled Plasmons

Florian Schertz,[1,*] Marcus Schmelzeisen,[2,3] Maximilian Kreiter,[2] Hans-Joachim Elmers,[1] and Gerd Schönhense[1]

[1]*Institut für Physik, Universität Mainz, Staudinger Weg 7, D-55099 Mainz, Germany*
[2]*Max Planck Institut für Polymerforschung, Ackermann Weg 10, D-55128 Mainz, Germany*
[3]*Center of Smart Interfaces, TU Darmstadt, Petersenstrasse 32, D-64287 Darmstadt, Germany*

(Received 17 January 2012; published 6 June 2012)

Field emission of electrons is generated solely by the ultrastrong near-field of strongly coupled plasmons without the help of a noticeable dc field. Strongly coupled plasmons are excited at Au nanoparticles in subnanometer distance to a Au film by femtosecond laser pulses. Field-emitted electrons from individual nanoparticles are detected by means of photoelectron emission microscopy and spectroscopy. The dependence of total electron yield and kinetic energy on the laser power proves that field emission is the underlying emission process. We derive a dynamic version of the Fowler–Nordheim equation that yields perfect agreement with the experiment.

DOI: 10.1103/PhysRevLett.108.237602 PACS numbers: 79.70.+q, 36.40.Gk, 79.60.−i

Since the discovery and fundamental comprehension of the external photoelectric effect by A. Einstein in 1905, electron emission from solid surfaces induced by photons has become a widely used method to study surface effects and the electron structure of solids. In addition to the common linear photoemission process, where the emitted electron captures the energy of a single photon, the development of pulsed lasers enabled multiphoton photoemission (nPPE, n referring to the number of photons involved in the emission process) [1,2], relying on the high photon density per pulse and providing additional information on unoccupied electron states. Using pump-probe schemes, time-resolved experiments have been implemented to investigate electron dynamics [3,4].

Along with an increase of the laser fluence, above-threshold photoemission has been observed [5,6]. In this process, the emitted electrons collect the energy of more photons than necessary to overcome the work function of the solid. In addition, few-cycle laser pulses allow for the investigation of carrier-envelope phase effects of the emission process on the attosecond time scale [7,8]. At even higher photon intensity, the onset of field emission has been predicted [2], being of particular interest for applications, e.g., bright ultralow emittance pulsed electron sources usable for time-resolved electron microscopy [9]. However, the experimental realization of this regime for solid-state surfaces has not yet been proven. This is due to the fact that the necessarily huge laser intensity can easily exceed the damage threshold of the sample [10,11]. In addition, space-charge effects easily impede the precise measurement of the electron yield [12]. Electron emission from nanostructures partly avoids the abovementioned obstacles, benefiting from the near-field enhancement of excited plasmons that strongly increases the nPPE probability [13,14]. In order to approach the field emission regime, several groups studied electron emission from a metal tip with a curvature radius of several tens of nanometers, where a dc voltage was applied in addition to the laser excitation [8,15–19]. Increasing the dc voltage provoked a transition from a dominating nPPE process to the field emission of photoexcited electrons.

In contrast to previous studies, we report on the field emission of electrons that are solely emitted by the ultrastrong oscillating near-field that is generated by a coupled plasmonic structure. The near-field is excited in the subnanometer gap between a Au nanoparticle and a Au plane (nanoparticle-on-plane, NPOP) [20–22].

A sketch of the investigated sample is shown in Fig. 1(a). The preparation procedure was reported in detail by Schmelzeisen *et al.* [23]. A Si(111) surface was capped with a 1-nm thick Cr seed and a 50-nm thick Au film. Then, the sample was immersed into a solution containing the organic molecule cysteamine, which thereupon bound to the Au surface, constituting a self-assembled monolayer (SAM). In the final step, Au nanoparticles (≈ 90 nm diameter) [23] were placed onto the SAM. The SAM served as a spacer between the Au nanoparticles and Au film, forming a well-defined gap. The simulated field distribution around a NPOP is shown in Fig. 1(b) [24]. The photoemission experiments were conducted under ultrahigh vacuum conditions ($p \approx 10^{-9}$ mbar). The optical excitation was induced by p-polarized light of a Ti:Sa femtosecond laser (MaiTai Spectra-Physics, 80 MHz repetition rate, pulse width $\sim$100 fs, max. $\sim$7 nJ/pulse) in the wavelength range of 750–850 nm. The illuminated area ($> 10^4$ μm^2) was much larger than the detection area ($< 5 \times 10^2$ μm^2), ensuring a uniform illumination of the analyzed NPOPs. The emitted electrons were imaged by a photoemission electron microscope. A retarding field analyzer (RFA) operates as a high-pass energy filter with an energy resolution of 250 meV. A CCD camera converted the light of the fluorescence screen behind the RFA into digital information.

In order to identify the underlying electron emission process, we analyze the dependence of the total emission yield

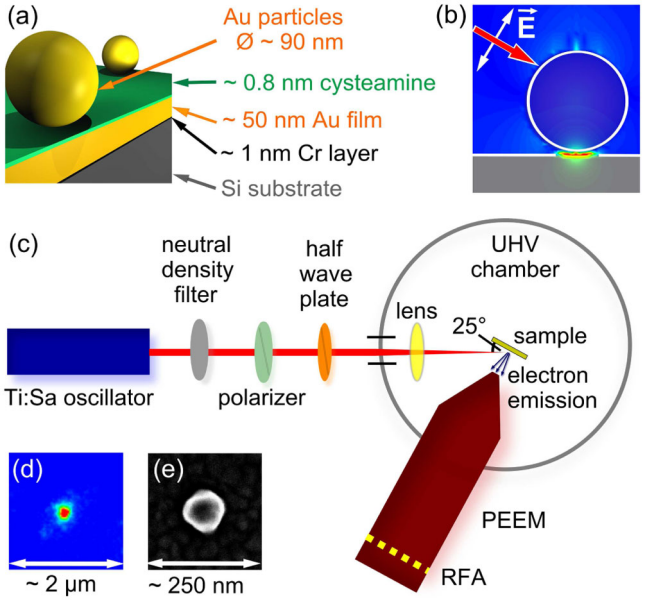

FIG. 1 (color online). (a) Sample structure, (b) calculated electric field distribution around a NPOP under gap resonance excitation, and (c) schematic setup of the gap resonance induced electron emission experiment by means of fs-laser excitation and photoemission electron microscopy detection, (d) PEEM- and (e) SEM- image of the identical NPOP.

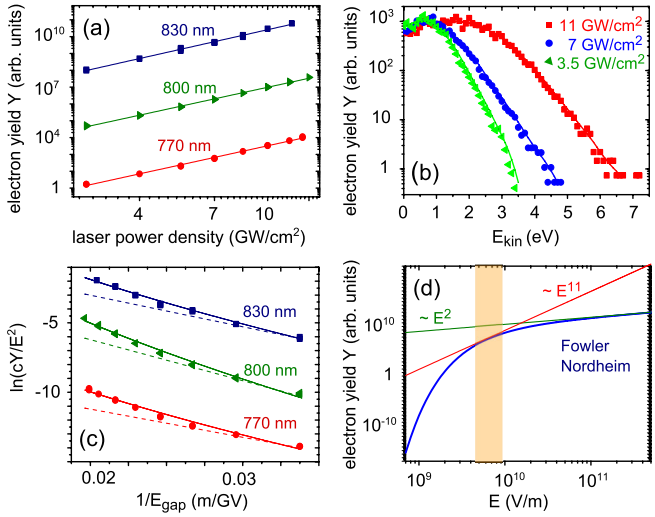

FIG. 2 (color online). (a) Total electron yield vs laser power density from an individual NPOP. The slopes of the fitted straight lines indicate a power law with an exponent of $n = 5.6(1)$ independent of the wavelength. An offset for the data was adopted for better visibility. The laser power density refers to the incident intensity; i.e., plasmonic enhancement is not considered. (b) Electron yield versus kinetic energy for the indicated laser power densities at 780 nm. (c) FN plot for the identical data as in (a). The solid curves indicate a fit to the modified FN equation [Eq. (2)]. The dashed lines illustrate the FN equation for static fields. (d) Double-logarithmic representation of the FN-behavior (blue curve). The straight green and red lines indicate power laws $n = 1$ and $n = 5.5$, respectively, ($Y \propto P^n \propto E^{2n}$, $n = 5.5$).

on the laser power density [Fig. 2(a) and 2(c)] and the kinetic energy distribution of the emitted electrons [Fig. 2(b)].

In a nPPE process, the electron yield Y is proportional to the nth power of the incident laser intensity P, $Y \propto P^n$ [2]. Hence, a double-logarithmic representation reveals the corresponding order from the slope in the Y vs P plot. Our result of $n = 5.5$ indicates a fractional value of n. We measured the workfunction Φ of the Au surface covered by a SAM of cysteamine molecules by illuminating the sample with light from a mercury arc lamp with a cutoff energy of 4.9 eV. In this case 1PPE from a sample area without NPOPs leads to a maximum kinetic energy of 0.9 eV, resulting in $\Phi = 4.0$ eV. Three photons (energy per photon ~1.55 eV) are needed to overcome the work function. Thus a 3PPE process is expected to be the prevailing photoemission process, i.e., we expect $n = 3$ instead of the measured $n = 5.5$. Therefore, the observed power dependence of the total electron yield is at variance with the model of nPPE. Also, above-threshold photoemission can be excluded, because it is clearly dominated by the lowest possible order [6,18].

An additional argument against nPPE is given by the missing energy in the kinetic energy distribution of the emitted electrons. For nPPE, the kinetic energy of an emitted electron is given by $E_{\mathrm{kin}} = nh\nu - E_b - \Phi$ (E_b: binding energy). The maximum kinetic energy of the emitted electrons stemming from the Fermi edge ($E_b = 0$) is expected to reach $E_{\mathrm{kin}} = nh\nu - \Phi$ independent of the laser power density. For a 6PPE (5PPE) process, laser pulses with a wavelength of 780 nm result in a maximum kinetic energy of 5.5 eV (3.9 eV). In order to compare with the observed energy distribution shown in Fig. 2(b), we introduce $E_{\mathrm{kin}}^{90\%}$ as the maximum kinetic energy of the 90th percentile of the electrons at a given laser power density, resulting in $E_{\mathrm{kin}}^{90\%}(3.5\,\mathrm{GW/cm^2}) = 1.4\,\mathrm{eV}$, $E_{\mathrm{kin}}^{90\%}(7\ \mathrm{GW/cm^2}) = 1.8$ eV and $E_{\mathrm{kin}}^{90\%}(12\ \mathrm{GW/cm^2}) = 3.0$ eV. In all cases, $E_{\mathrm{kin}}^{90\%}$ is smaller than the expected kinetic energy for a 6PPE (5PPE) process. A postemission acceleration process, as discussed below, can only increase the kinetic energy, thus leaving even less remaining energy for the initial photoemission process. Thus, the total electron yield and the energy distribution of the emitted electrons cannot be explained by a nPPE process.

A totally different emission mechanism is given by field emission, which occurs only in the presence of very strong electric fields. In the case of dc electric fields, the field emission results in a narrow energy distribution of emitted electrons, in contrast to our experimental results. Nevertheless, in the following we will show that the observed energy distribution can well be explained by a field emission model considering postemission acceleration. For discrimination between photoemission and field emission, Keldysh proposed the dimensionless parameter

$\gamma = \omega\sqrt{(2m\Phi)/(eE)}$ [25], where ω is the angular frequency, and E the electric field strength amplitude of the light, m is the mass and e the charge of the electron and Φ is the work function. Photoemission is favored for $\gamma > 1$ and field emission for $\gamma < 1$. Using our experimental parameters, we obtain a power density of $w \approx 6 \cdot 10^8$ W/cm^2 on the sample, corresponding to an electric field strength of $E_{\text{laser}} \approx 50$ MV/m. The electric field strength in the gap of the NPOP is enhanced by plasmon coupling. We performed numerical simulations using CST MICROWAVE STUDIO 2010 [24]. Considering a sphere on plane system with a sphere diameter and gap width similar to the ones used in the experiment, we obtained an enhancement factor of 10^3. Therefore, the electric field strength in the gap is $E_{\text{gap}} \approx 50$ GV/m and thus, the Keldysh parameter results in $\gamma \approx 0.2$, indicating the strong field regime where field emission is favored.

In the case of static electric fields, the total electron yield varies in dependence on the electric field strength E according to the Fowler–Nordheim (FN) equation [17,26]

$$J = aE^2 \exp(-b/E) \tag{1}$$

with a and b denoting constants for a given experimental geometry. A comparatively large dc field of several V/nm has to be applied to reach the field emission regime. In our experimental setup, the dc field generated by the PEEM extractor (objective lens) is 3 orders of magnitude smaller ($E_{\text{ext}} = 2$ mV/nm). Hence, the electron tunneling is entirely induced by the plasmon-enhanced optical near-field. In order to illustrate the field dependence according to Eq. (1), we present experimental data in the FN-plot [Fig. 2(c)]. In this plot the field dependence of Eq. (1) shows up as a straight line. Indeed, the experimental data show an almost linear decrease. The remaining systematic deviations are explained by the fact that the field is oscillating instead of being constant. Within one oscillation of a laser cycle, electric field values between $E_{\text{min}} = 0$ and $E_{\text{max}} = E_{\text{gap}}$ contribute. Negative values of E are not considered as no electron emission occurs in this case. In order to describe the total electron yield Y for varying electric field strength, we integrate the partial currents generated by the time-dependent field $E(t)$:

$$Y = \frac{1}{T}\int_0^{T/2} J dt = \frac{1}{T}\int_0^{T/2} a^* E^2(t) \exp(-b^*/E(t)) dt \tag{2}$$

The time-dependence of the electric field is described by $E(t) = E_0 \cdot \sin(\omega t)$. A numerical fit to this function is shown in Fig. 2(c) (solid line). Instead of the original FN-equation [dashed line in Fig. 2(c)], Eq. (2) reproduces the positive curvature of the experimental data, thus confirming this ansatz.

In the following, we discuss the reason for the linear behavior in the double logarithmic plot of Fig. 2(a). Experimental limitations confine the investigated interval of the electric field strength considerably. Because of the strong decrease of the electron yield with decreasing laser power density, it is impossible to measure the total electron yield when the intensity is reduced by more than a factor of 4 from the maximum value, corresponding to a reduction of the electric field strength by a factor of 2. To ensure an appropriate data analysis with justifiable statistical conditions, the exposure time must be enhanced by a factor of $\sim$50, if the excitation intensity is decreased by a factor of 2, due to $2^{5.5} \approx 50$. Instabilities in our experimental setup on a time-scale of hours rule out a further reduction of the laser intensity. In the investigated interval of the electric field, the FN-equation can be approximated by a power law as demonstrated in Fig. 2(d). For large electric field values, Eq. (1) is approximated by $Y \propto P \propto E^2$, i.e. $n = 1$. At lower electric field values the exponent n increases to infinity. For reasonable experimental conditions near $E = 50$ GV/m the FN-behavior is approximated by $Y \propto P^{5.5} \propto E^{11}$, i.e. $n = 5.5$, in nice agreement with the experimental observation.

Field emission alone does not explain the kinetic energy distribution displayed in Fig. 2(b) and their pronounced dependence on the laser power density. Larger intensities generate an increasing contribution of electrons with high kinetic energy. Electrons with energies up to $E_{\text{kin}}^{\text{max}} \approx 7$ eV are emitted at a power density of 11 GW/cm^2. We would like to emphasize, that space-charge effects, causing a spread of kinetic energy of the electrons due to Coulomb repulsion [12], do not play any role here, since the average electron yield from one NPOP per pulse is less than one.

High kinetic energies can be explained by the ponderomotive force of an oscillating and strongly inhomogeneous electric field, expelling a charged particle out of the region of strong fields [7,27–29]. The ponderomotive force $F_{\text{pond}} = -\nabla U_{\text{pond}}$ acts on the electrons after the emission, $U_{\text{pond}} = (e^2E^2)/(4m\omega^2)$ being the quiver energy of a charged particle in an oscillating, inhomogeneous electric field E. The negative sign indicates, that the electrons are accelerated in the direction of weaker electric field. This effect has been observed in several studies for SPP excitation on metal films [7,27–29], constituting electrons with kinetic energies up to the keV-range [29]. In our experimental setup, the kinetic energies are expected to be much lower, since the energy gain depends both on the pulse duration of the laser and the spatial distribution of the ponderomotive potential. The enhancement of the near-field of a NPOP with a subnanometer gap between particle and plane is strongly localized in the gap, see Fig. 1(b). Therefore, the gradient of the ponderomotive potential is large in the vicinity of the gap and rapidly decreasing with increasing distance from the gap, resulting in a smaller energy gain.

As an estimate, we calculate the energy gain of an electron on its way from the gap to the homogenous field regime using the field distribution shown in Fig. 1(b). For the maximum laser power density, the calculated

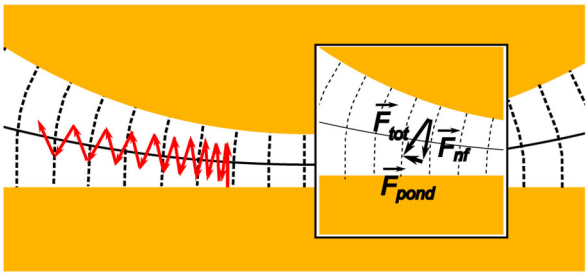

FIG. 3 (color online). Supposed electron trajectories in the gap between Au nanoparticle and Au plane (schematic). The inset shows the underlying forces acting on the electron at a given instant of time. The plasmon-enhanced optical near-field gives rise to an oscillation of the electron caused by $\boldsymbol{F}_{\mathrm{nf}}$. The ponderomotive force $\boldsymbol{F}_{\mathrm{pond}}$ superimposes the oscillation, resulting in a total force $\boldsymbol{F}_{\mathrm{tot}} = \boldsymbol{F}_{\mathrm{nf}} + \boldsymbol{F}_{\mathrm{pond}}$ causing a drift towards the low-field region, i.e., outside the gap.

kinetic energy results in 10 eV, being in a good agreement with the observed maximum energy gain of ~7 eV.

The excitation of a plasmon does not only enhance the near-field, but also the scattering efficiency to the far-field [30]. The emitted electrons might interact with the light radiated into the far-field, affecting, e.g., their kinetic energy distribution. However, we have shown in a recent study that the resonances induced with the given experimental conditions are dark modes; i.e., no scattering occurs in this wavelength regime [31].

In Fig. 3, the calculated electron trajectories are sketched. The ponderomotive potential does not only accelerate the electrons but also directs them out of the gap region around the nanoparticle towards the region of the constant small extractor field. Consequently, the ponderomotive potential enables the experimental study of the electric near-field by means of PEEM, even if the direct access to the emission region is shielded by components of the sample. Therefore, PEEM is a superior method to analyze the strong coupling of plasmons via ultrasmall gaps, to which the experimental access by means of conventional tip-based near-field techniques (e.g., scanning near-field optical microscopy, SNOM) is unfeasible.

Strongly coupled plasmons generate ultrastrong near-fields. We have shown that these ultrastrong fields can be utilized to extract electrons from solid-state surfaces by a field emission process. The field emission process deviates from static field emission because of the oscillation of the electric near-field and can be described by a modified Fowler-Nordheim behavior. Electrons can be extracted even from buried spots due to the ponderomotive acceleration which makes the process very useful for the characterization of coupled plasmonic systems of arbitrary geometry. Since the coupled plasmonic structure gathers the incident energy from the light wave and focuses it to a region far below the optical diffraction limit, ultrastrong fields can be achieved even with moderate excitation intensities. Therefore, the plasmonic field emission process from coupled plasmonic systems described here opens a path to investigate electron emission under unprecedented large electric fields that are far above the destruction level for plane wave illumination.

The financial support from Deutsche Forschungsgemeinschaft through SPP 1391 and SFB 625 is gratefully acknowledged. We thank Martin Aeschlimann for fruitful discussions.

*scherfl@uni-mainz.de

[1] S. Anisimov, V. Benderskii, and G. Farkas, Sov. Phys. Usp. **20**, 467 (1977).
[2] G. Ferrini, F. Banfi, C. Giannetti, and F. Parmigiani, Nucl. Instrum. Methods Phys. Res., Sect. A **601**, 123 (2009).
[3] H. Petek and S. Ogawa, Prog. Surf. Sci. **56**, 239 (1997).
[4] G. Schönhense, H.-J. Elmers, S. A. Nepijko, and C. M. Schneider, Adv. Imaging Electron Phys. **142**, 159 (2006).
[5] M. Aeschlimann, C. Schmuttenmaer, H. Elsayedali, R. Miller, J. Cao, Y. Gao, and D. Mantell, J. Chem. Phys. **102**, 8606 (1995).
[6] F. Banfi, C. Giannetti, G. Ferrini, G. Galimberti, S. Pagliara, D. Fausti, and F. Parmigiani, Phys. Rev. Lett. **94**, 037601 (2005).
[7] S. E. Irvine, P. Dombi, G. Farkas, and A. Y. Elezzabi, Phys. Rev. Lett. **97**, 146801 (2006).
[8] M. Krüger, M. Schenk, and P. Hommelhoff, Nature (London) **475**, 78 (2011).
[9] J. S. Kim, T. LaGrange, B. W. Reed, M. L. Taheri, M. R. Armstrong, W. E. King, N. D. Browning, and G. H. Campbell, Science **321**, 1472 (2008).
[10] J. P. Girardeau-Montaut and C. Girardeau-Montaut, Phys. Rev. B **51**, 13560 (1995).
[11] S. A. Hilbert, A. Neukirch, C. J. G. J. Uiterwaal, and H. Batelaan, J. Phys. B **42**, 141001 (2009).
[12] N. M. Buckanie, J. Goehre, P. Zhou, D. von der Linde, M. Horn-von Hoegen, and F.-J. M. z. Heringdorf, J. Phys. Condens. Matter **21**, 314003 (2009).
[13] T. Tsang, T. Srinivasan-Rao, and J. Fischer, Phys. Rev. B **43**, 8870 (1991).
[14] M. Cinchetti, A. Gloskovskii, S. A. Nepjiko, G. Schönhense, H. Rochholz, and M. Kreiter, Phys. Rev. Lett. **95**, 047601 (2005).
[15] C. Ropers, D. R. Solli, C. P. Schulz, C. Lienau, and T. Elsaesser, Phys. Rev. Lett. **98**, 043907 (2007).
[16] R. Bormann, M. Gulde, A. Weismann, S. V. Yalunin, and C. Ropers, Phys. Rev. Lett. **105**, 147601 (2010).
[17] P. Hommelhoff, Y. Sortais, A. Aghajani-Talesh, and M. A. Kasevich, Phys. Rev. Lett. **96**, 077401 (2006).
[18] M. Schenk, M. Krüger, and P. Hommelhoff, Phys. Rev. Lett. **105**, 257601 (2010).
[19] H. Yanagisawa, C. Hafner, P. Dona, M. Klöckner, D. Leuenberger, T. Greber, J. Osterwalder, and M. Hengsberger, Phys. Rev. B **81**, 115429 (2010).
[20] P. Aravind and H. Metiu, Surf. Sci. **124**, 506 (1983).
[21] A. Rueda, M. Stemmler, R. Bauer, K. Müllen, Y. Fogel, and M. Kreiter, New J. Phys. **10**, 113001 (2008).
[22] P. Nordlander and E. Prodan, Nano Lett. **4**, 2209 (2004).

[23] M. Schmelzeisen, J. Austermann, and M. Kreiter, Opt. Express **16**, 17826 (2008).
[24] T. Weiland, Int. J. Numer. Modell. Electron. Networks Devices Fields 9, 295 (1996); http://www.cst.com.
[25] L. Keldysh, Sov. Phys. JETP **20**, 1307 (1965).
[26] V. T. Binh, N. Garcia, and S. Purcell, Adv. Imaging Electron Phys. **95**, 63 (1996).
[27] J. Kupersztych, P. Monchicourt, and M. Raynaud, Phys. Rev. Lett. **86**, 5180 (2001).
[28] J. Kupersztych and M. Raynaud, Phys. Rev. Lett. **95**, 147401 (2005).
[29] S. E. Irvine and A. Y. Elezzabi, Appl. Phys. Lett. **86**, 264102 (2005).
[30] Z. J. Zhang, R. W. Peng, Z. Wang, F. Gao, X. R. Huang, W. H. Sun, Q. J. Wang, and M. Wang, Appl. Phys. Lett. **93**, 171110 (2008).
[31] F. Schertz, M. Schmelzeisen, R. Mohammadi, M. Kreiter, H.-J. Elmers, and G. Schönhense, Nano Lett. **12**, 1885 (2012).